

Research Paper

Cite this article: Hyvernaud J, Reineix G, Negrier R, Andrieu J, Lalande M, Couderc V (2020). Optoelectronic generation of transient waveforms for UWB radars with rejected frequencies. *International Journal of Microwave and Wireless Technologies* **12**, 543–550. <https://doi.org/10.1017/S1759078720000288>

Received: 9 November 2019

Revised: 11 March 2020

Accepted: 11 March 2020

First published online: 7 April 2020

Key words:


Ultra wideband radar; radiofrequency interference; optoelectronic devices; power semiconductor switches; signal generators

Author for correspondence:

Jeremy Hyvernaud

E-mail: jeremy.hyvernaud@unilim.fr

Optoelectronic generation of transient waveforms for UWB radars with rejected frequencies

Jeremy Hyvernaud¹ , Gwenael Reineix¹, Romain Negrier¹, Joel Andrieu¹, Michele Lalande¹ and Vincent Couderc²

¹Xlim Laboratory, Antennas and Signals, University of Limoges, France and ²Xlim Laboratory, Photonics, University of Limoges, France

Abstract

In this paper, a new design of an optoelectronic system for transient waveforms shaping, with a selection of rejected frequencies, is presented. The generation of short pulses is performed with several optoelectronic generators using photoconductive semiconductor switches (PCSS) operating in linear switching mode and triggered via a laser pulse. With the appropriate number of generators, the system generates a spectrum ranging from 300 MHz to 3 GHz, with rejected frequencies at 900 MHz and 1.8 GHz. A PCSS characterization has been set up to determine the necessary parameters for the establishment of an optoelectronic generator model on Keysight Advanced Design System software (ADS). Experimental tests have been realized using measurement benches to compare the simulated and measured signals.

Introduction

Over the past years, many studies are interested in ultra wideband (UWB) technologies. Areas such as life detection [5] are, for example, actively investigated. Indeed, UWB waveforms allow, with their low-frequency spectrum, to cross walls [11] or rubble during an earthquake. Systems in development have the ability to measure torso deformity to deduce the respiratory or heart rate, as well as the vital constants of patients [8]. UWB signals are also used in the context of soil penetration [2] for the detection of buried objects like mines.

However, one of the major disadvantages of UWB signals is related to the widespread spectrum that causes interference with other narrow band systems. Research shows the effects on existing UMTS [3], OFDM transmission [13] or GSM [1] systems. An UWB spectrum with rejected frequencies would then have a considerable advantage in limiting or suppressing interference. Some existing solutions are commonly proposed such as notch filters [6, 7] or frequency-selective surfaces [4, 9, 16].

The proposed solution in this paper resides on an innovative method of transient shaping to respect a given spectral template. The main difference between this solution and those presented previously is that the unwanted frequency components are not directly generated, preventing possible reflection problems caused by filtering. To create the desired spectrum, several optoelectronic generators have been used. These generators include photoconductive semiconductor switches (PCSS), operating in linear mode, adapted to the generation of particular waveforms of several kilovolts with a rise time in picoseconds or nanoseconds [12, 14]. Furthermore, PCSS are particularly well suited with very low jitter response and insulation between the electrical and optical commands.

Each optoelectronic generator generates a damped sinusoid whose FFT corresponds to a part of the total spectrum. The management of the synchronization of each waveform allows the formation of the desired spectrum. The development of this UWB system is based on an attenuation criterion of at least 20 dB for the two selected rejected frequencies (900 MHz and 1.8 GHz).

The paper is developed as follows: section “PCSS characterization” presents the optoelectronic generators principle and a characterization of PCSS; section “System model” describes the system model that focuses on the development and the optimization of damped sinusoids optoelectronic generators; section “Experimental setups and results” shows the experimental setups and results while section “Conclusion” concludes the paper.

PCSS characterization

Optoelectronic generator with one PCSS

The optoelectronic generator operation is based on the frozen wave generator principle. It consists of a PCSS placed at one of the ends of a microstrip line, equivalent to a capacitive element

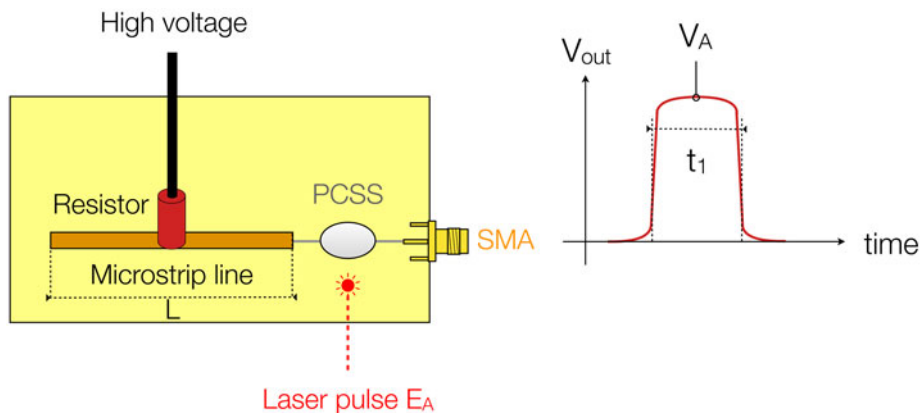
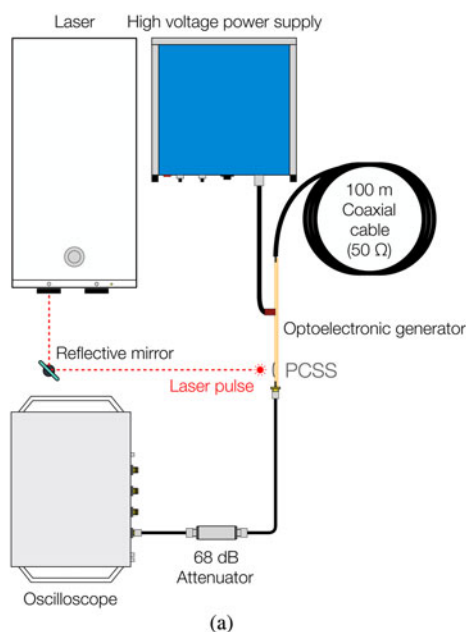
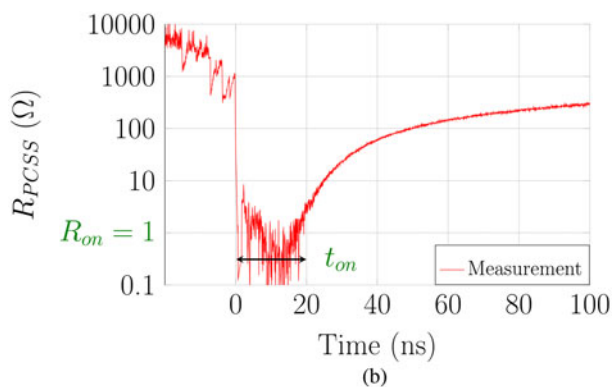


Fig. 1. Optoelectronic generator with one PCSS.



(a)



(b)

Fig. 2. (a) Measurement bench to characterize the PCSS. (b) Evolution of R_{PCSS} after a laser pulse E_A of $10\mu\text{J}$ at a bias voltage of 400 V.

(see Fig. 1). This microstrip line is charged via a resistor connected to a high voltage DC power source, for a relatively long time. The PCSS is then illuminated by infrared pulses provided by a laser source. The incident optical energy creates electron hole-pairs, greatly reducing the PCSS impedance and leading to an ultrafast release of the high voltage static field, confined to

the microstrip line, in the form of a square electrical pulse. After some time, the recombination of the charge carriers naturally occurs in the PCSS and induces its electrical reopening. The duration of the electrical output signal t_1 depends on the microstrip line length L , while the peak level V_A of the pulse depends on the applied bias voltage and optical energy E_A .

Experimental setup

PCSS used are the GP02-20 model sold by VISHAY. They are made of silicon and have a maximum bias voltage of 2 kV. The characterization set up makes it possible to determine the value of the on-state resistance R_{on} after a laser pulse, as well as the time t_{on} during which the PCSS remains electrically closed (the time before the beginning of the charge carrier recombination). The knowledge of R_{on} and t_{on} ensures the establishment of a correct PCSS model for simulations.

The optoelectronic generator depicted in Fig. 1 has been used to measure these parameters. The PCSS is illuminated by infrared pulses of 80 ps, delivered by an Ekspla PL2250 laser source with a wavelength of 1064 nm and a repetition rate of 1 Hz. A long 50 Ω coaxial cable of 100 m (type RG58CU, $\varnothing 4.95$ mm, conductor 19/0.19 mm, NVP 0.66), terminating in a circuit open, is added at the end of the microstrip line of the optoelectronic generator (see Fig. 2(a)). With this cable, the reflected wave takes a long time to return to the PCSS. This procedure illustrates the recombination phenomenon and a relationship between the bias voltage, the optical energy of the laser, and the effect on the R_{on} and t_{on} parameters has been established. The R_{PCSS} impedance can be calculated using (1).

$$R_{PCSS} = \frac{(V_b - V_{out}) \cdot Z_{load}}{V_{out}} - Z_{source} \quad (1)$$

V_b is the bias voltage, V_{out} is the measured voltage at the output of the SMA connector, Z_{source} is the impedance of the microstrip line of the optoelectronic generator (50 Ω) and Z_{load} is the impedance of the load (50 Ω of the oscilloscope). The evolution of the measurement of the resistance of the PCSS is plotted in Fig. 2(b) with a fixed bias voltage of 400 V. In the closed state, R_{on} is equal to 1 Ω . The time t_{on} when the PCSS remains electrically closed is a function of the amount of optical energy E_A emitted. For example, this gives the possibility of generating signals with a duration of 20 ns for 10 μJ .

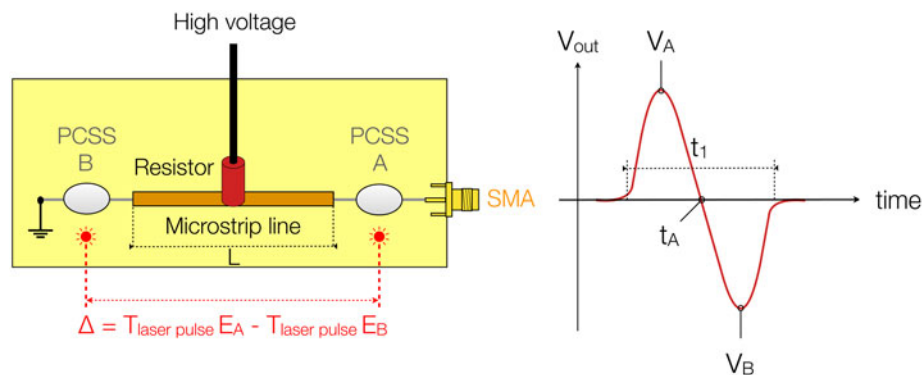


Fig. 3. Optoelectronic generator with two PCSS.

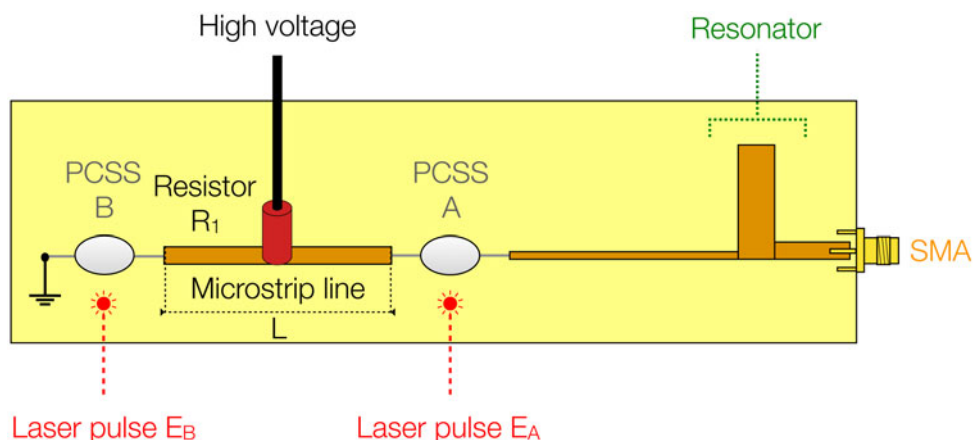


Fig. 4. Damped sinusoids optoelectronic generator.

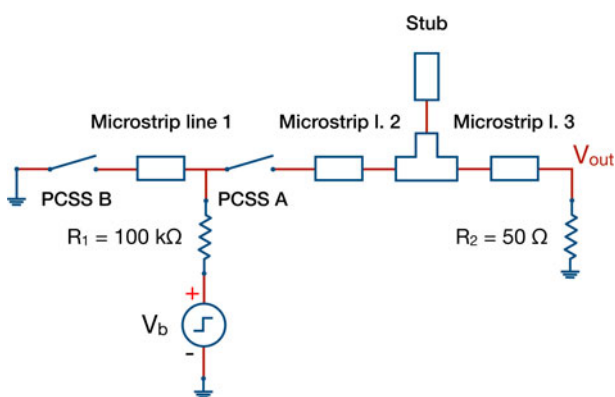


Fig. 5. Keysight ADS model of the damped sinusoids optoelectronic generator.

System model

Optoelectronic generator with two PCSS

It is also possible to design optoelectronic generators with two PCSS placed on either side of the microstrip line (see Fig. 3). An infrared pulse on both PCSS drops their impedance and allows the ultrafast release of the static high voltage field, confined on the microstrip line, in the form of a progressive wave and a regressive wave. The reflection of the regressive wave at the

Table 1. Parameters of the three damped sinusoids

Signal	Center frequency f_c	Q factor	P-P magnitude
1	786 MHz	8	50 V
2	1.47 GHz	8	84 V
3	2.46 GHz	8	141 V

PCSS B placed near the ground induces an inversion of its polarity. A superposition of these two waves forms, at the output, a bipolar electric pulse. The duration of the electrical output signal t_1 depends on the microstrip line length L , whereas the bias voltage and the optical energies E_A and E_B applied on the PCSS allow to respectively modulate the peak levels of the positive part V_A and the negative part V_B of the electric pulse. It is also possible to shift the time when the inter-alternating transition front t_A appears by acting on the trigger times $T_{laser-pulse-A}$ and $T_{laser-pulse-B}$ of the infrared pulses.

From a bipolar electrical pulse, and with the aim of tending toward a damped sinusoidal signal, the optoelectronic generator with two PCSS illustrated in Fig. 3 has been modified (see Fig. 4). Following PCSS A, a microstrip line associated with a stub, as presented in [17], introduces the resonance phenomenon. The bipolar electrical pulse is thus maintained over time to form a damped sinusoid.

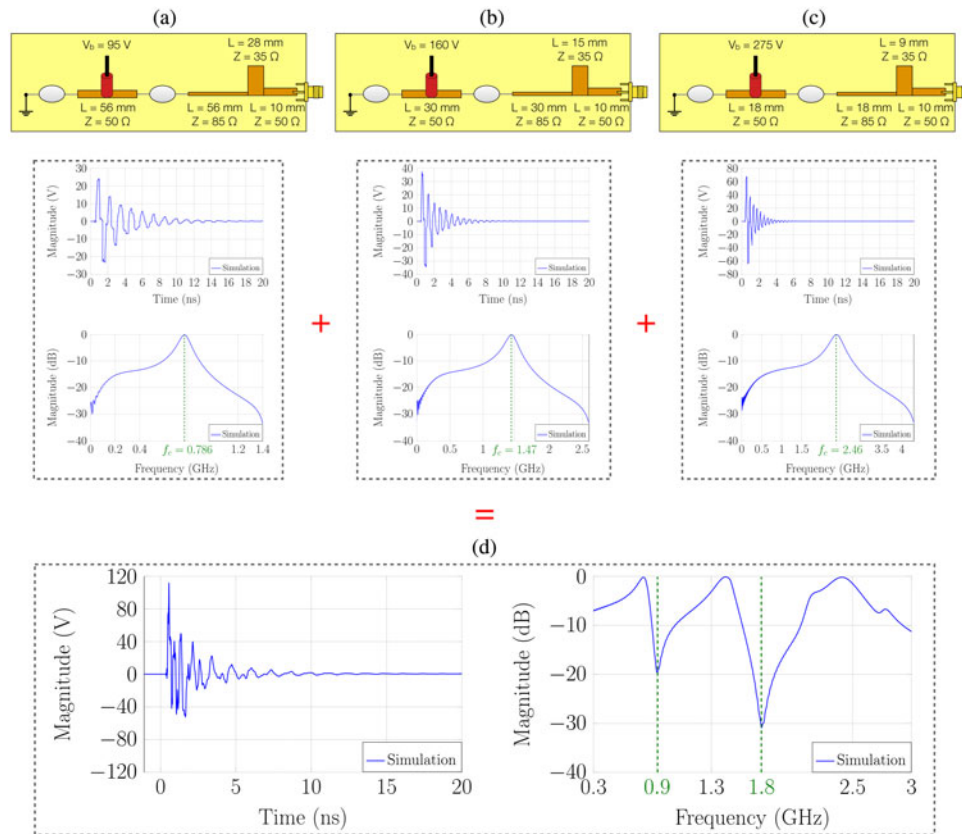


Fig. 6. Transient and spectral shapes of the output signal (a) of the first generator with $f_c = 786$ MHz; (b) of the second generator with $f_c = 1.47$ GHz; (c) of the third generator with $f_c = 2.46$ GHz; (d) simulated global spectrum with the two rejected frequencies and the associated transient shape.

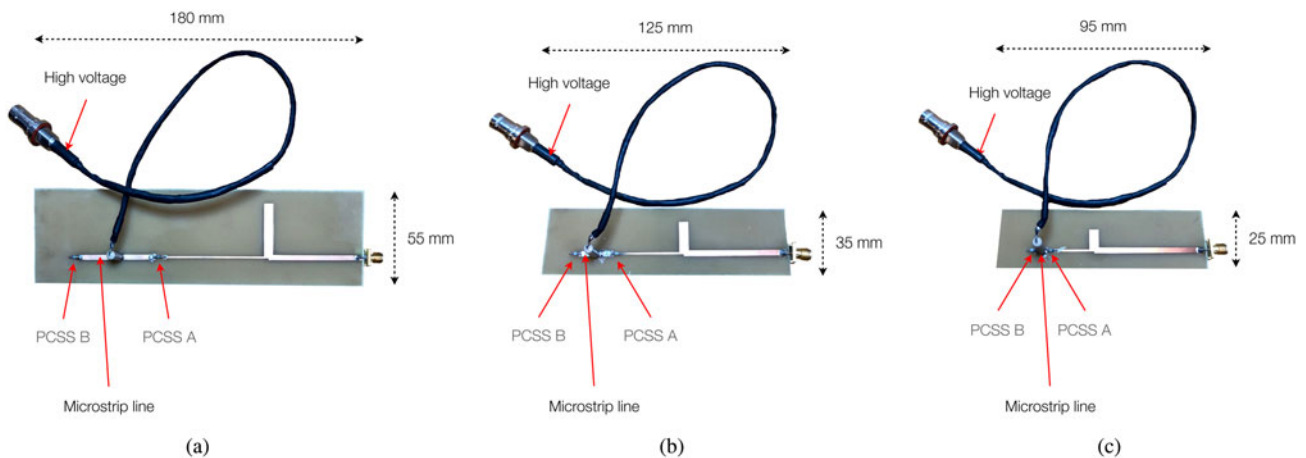


Fig. 7. Realization of three damped sinusoids optoelectronic generators (a) at a center frequency of 786 MHz; (b) at a center frequency of 1.47 GHz; (c) at a center frequency of 2.46 GHz.

Figure 5 represents the realized model with Keysight ADS software of the damped sinusoids optoelectronic generator where the microstrip lines and the stub have been implemented. Both PCSS are considered switches with an on-state resistance of 1Ω in the closed state, matching the impedance value of the components after a laser pulse (see Fig. 2(b)). Bias voltage applied to the microstrip line between the PCSS is modeled by a pulse source and the large value of the resistor R_1 prevents from any reflection. The output signal, measured on the load resistor R_2 , is acquired

once the microstrip line is fully charged and after closing the two switches. The substrate used is epoxy resin (FR-4) which has a thickness of 1.5 mm, a relative dielectric constant of 4.3 and a dielectric loss tangent of 0.02.

Simulations

To create a spectrum over a wide frequency band [300 MHz–3 GHz], and to obtain at least an attenuation of 20 dB for the

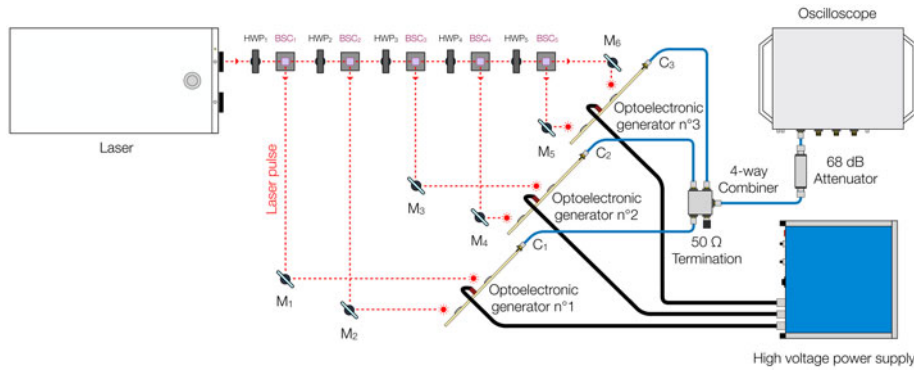


Fig. 8. Measurement bench to generate the global spectrum with a combiner; M: Reflective Mirror; HWP: Half Wave Plate; BSC: Beam Splitter Cube; C: Cable.

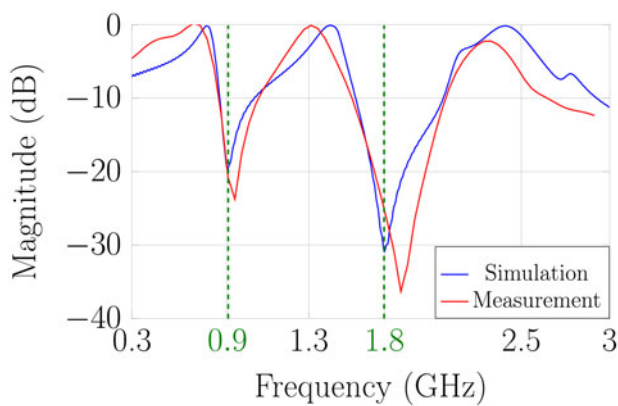


Fig. 9. Comparison between simulated and measured spectra.

two selected rejected frequencies (900 MHz and 1.8 GHz which correspond to European GSM frequencies), the transient pulse is chosen as the sum of three damped sinusoids by an optimization algorithm [15]. Center frequency, peak-to-peak magnitude, and Q factor of each sinusoid must be optimized in order to respect the desired spectral shape. The results of the algorithm are listed in Table 1.

Each of these signals will be generated by a different damped sinusoids optoelectronic generator. A transient optimization (10 ps time step) of the output shape of the Keysight ADS model in Fig. 5 has been used to calculate the length and impedance of the microstrip lines. Figure 6 shows the geometry of the three determined optoelectronic generators to obtain the signals of Table 1. The summation of the three spectra makes it possible to create the global spectrum containing the two rejected frequencies (see Fig. 6(d)). In simulation, the attenuation for the first frequency at 900 MHz is 20 dB while the attenuation for the second frequency at 1.8 GHz is 30 dB.

Experimental setups and results

The three damped sinusoids optoelectronic generators have been realized with 1.5 mm thick epoxy resin substrate (FR-4) to validate the simulation (see Fig. 7). The summation of the output signals of each generator has been done in two different ways.

Summation with a combiner

Figure 8 shows the measurement bench used to generate the global spectrum by summation of the three signals with a combiner (ZFRSC-4-842-S+). An Ekspla PL2250 laser source delivers 80 ps pulses with a repetition rate of 10 Hz in the infrared range

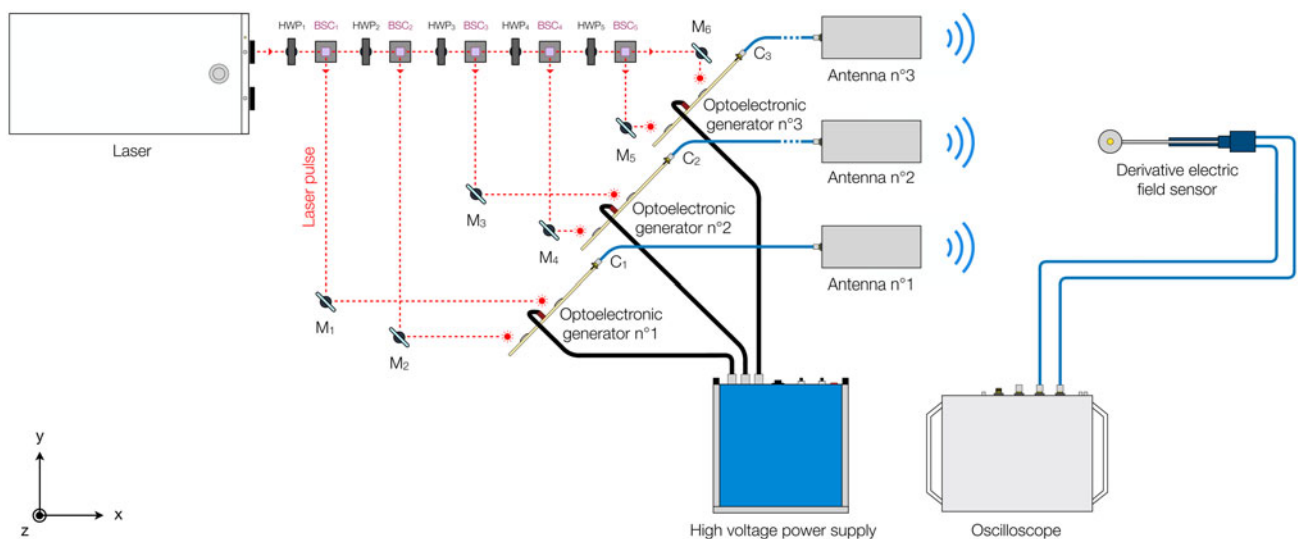


Fig. 10. Measurement bench to generate the global spectrum with antennas; M: Reflective Mirror; HWP: Half Wave Plate; BSC : Beam Splitter Cube; C: Cable.

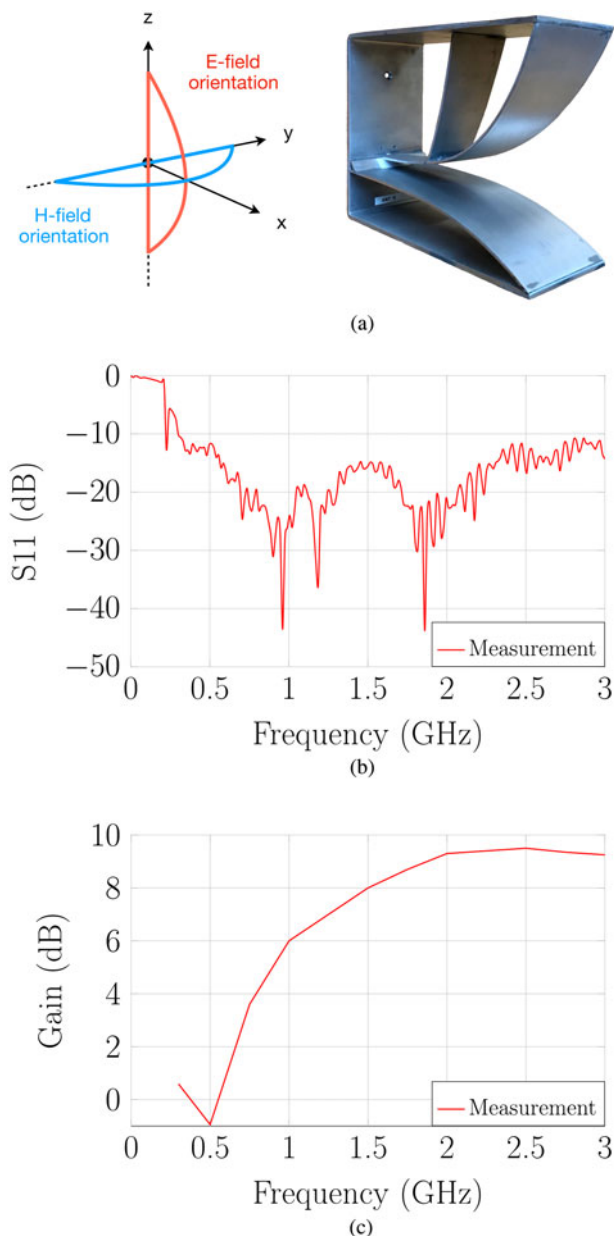


Fig. 11. (a) Antenna; (b) reflection coefficient; (c) realized gain in the main direction.

(1064 nm). The laser beam is separated into two adjustable parts using a half wave plate ($HWP_1, HWP_2, \dots, HWP_5$) coupled to a beam splitter cube ($BSC_1, BSC_2, \dots, BSC_5$). The distribution of the optical energy between the beams is adjusted to obtain the same illumination of the six PCSS. Adjustable mirrors (M_1, M_2, \dots, M_6) are arranged after the splitter cube to equalize the length of the different optical paths. Each damped sinusoids optoelectronic generator is powered by a voltage power supply and is connected to a four-way combiner; the fourth unused input has been connected to a 50Ω termination. To avoid phase shift before the signals are summed, the three cables (C_1, C_2 , and C_3) are paired in phase at $\pm 2^\circ$. For the acquisition of the output signal, a Barth attenuation chain of 68 dB and a Keysight DSOX92004Q Infiniium oscilloscope have been used. It operates in real time with an 8 GHz bandwidth and an acquisition time of 20 GSa/s.

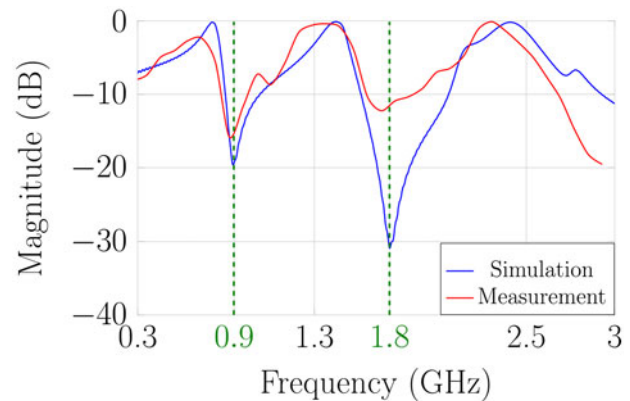


Fig. 12. Comparison between simulated and measured spectra.

The simulated and experimental results are compared in Fig. 9. The good superposition of the curves allows to validate the Keysight ADS model. On the frequency band [300 MHz–3 GHz], two rejected frequencies have been obtained with attenuation levels in line with expectations. The first rejected frequency at 900 MHz has an attenuation of 20 dB while the second at 1.8 GHz has an attenuation of 25 dB. A slight difference between the experimental and simulated center frequencies of each damped sinusoids optoelectronic generator is noticeable. The center frequency values are 703 MHz, 1.37 GHz, and 2.38 GHz instead of 786 MHz, 1.47 GHz, and 2.46 GHz. This is caused by the miniaturization of optoelectronic generators when the desired center frequency increases. The length of the PCSS pins then becomes less negligible and induces a frequency shift. The prospects for improvement will focus on establishing a better PCSS simulation model. It will then be possible to take into account the PCSS pins length, as well as the impedance difference caused by the welding of these components on the microstrip lines. This should help to solve the center frequency shift of each damped sinusoids optoelectronic generator.

Summation with an antenna by generator

Figure 10 shows the measurement bench used to generate the global spectrum by summation of the radiations of the three signals with antennas. The measurement bench is identical to that shown in Fig. 8 except that each damped sinusoids optoelectronic generator is connected to an antenna. The UWB antenna chosen for this application is based on the work of Koshelev [10] which combines a magnetic loop and the radiation mode of a traveling wave antenna (see Fig. 11(a)). With a height of 21 cm, a length of 30 cm and a width of 10 cm, this antenna has a very wide adaptation with a matching bandwidth at -10 dB between 300 MHz and 3 GHz (see Fig. 11(b)). Figure 11(c) shows that the realized gain in the main radiation direction is weak for low frequencies under 1 GHz and moderated/high for frequencies above. The spacing between each antenna is 30 cm. For the acquisition, a Montena SFE3-5G derivative electric field sensor has been placed at a distance of 8 m from the antennas. To visualize the experimental spectrum, the output signal acquired by the electric field sensor corresponding to the derivative of the field is integrated; an FFT is then applied.

The simulated and experimental results are compared in Fig. 12. Since the transfer function of the antennas has not been taken into account in the simulation, the geometry and the bias voltage of the damped sinusoids optoelectronic generators are no longer adapted to maintain the shape of the desired

global spectrum. Rejected frequencies are less attenuated: 15 dB at 900 MHz and 11 dB at 1.8 GHz. To better match the shape the Keysight ADS simulation must consider the antenna characteristics (in particular the gain evolution) to include their effects in the optimization of generator geometry.

Conclusion

Transient waveforms shaping with a selection of rejected frequencies have been demonstrated using three damped sinusoids optoelectronic generators. Optoelectronic generators operation has been first introduced; then a characterization of the used PCSS has been carried out to design an Keysight ADS model of the damped sinusoids optoelectronic generator. Measurement benches have been finally set up to compare the measured spectrum and thus validate the simulation. The desired goals have been achieved and there is a good agreement between the simulation and measurement results. A spectrum in the [300 MHz–3 GHz] frequency band with two rejected frequencies has been obtained, the first at 900 MHz with an attenuation of 20 dB, and the second at 1.8 GHz with an attenuation of 25 dB. For instance, GSM devices should therefore be resistant to interfering signals from radar system powered by this type of transient shaped waveforms.

Acknowledgments. The authors would like to thank the French Armament procurement Agency DGA, the French Alternative Energies and Atomic Energy Commission CEA and the New Aquitaine region for their fundings.

References

1. **Abdullah A, Ahmad A, Sauti MS, Erana Y, Shaaya SA and Mustafa IS** (2008) Simulation study of UWB interference effects on gsm 900 system. *2008 6th National Conference on Telecommunication Technologies and 2008 2nd Malaysia Conference on Photonics, Putrajaya, Aug 2008*, pp. 386–391.
2. **Ahmed A, Zhang Y, Burns D, Huston D and Xia T** (2016) Design of uwb antenna for air-coupled impulse ground-penetrating radar. *IEEE Geoscience and Remote Sensing Letters*, **13**, 92–96.
3. **Al-Adwany MAS, Najim EH, Ali AB and Younis AM** (2010) A study on the effect of uwb interference on downlink umts system. *2010 1st International Conference on Energy, Power and Control (EPC-IQ), Basrah, Nov 2010*, pp. 107–110.
4. **Bouslama M, Traii M, Denidni TA and Gharsallah A** (2016) Beam-switching antenna with a new reconfigurable frequency selective surface. *IEEE Antennas and Wireless Propagation Letters*, **15**, 1159–1162.
5. **Dou M and Zhang W** (2018) Improved ranging method for life detection using ultra-wide band impulse radar. *Journal of Engineering*, **2018**, 1375–1383.
6. **Hammed RT and Mirshekar-Syahkal D** (2013) Multiple band rejection notches in miniaturized uwb fifth-order filter using e-shape microstrip structures. *2013 IEEE 13th Topical Meeting on Silicon Monolithic Integrated Circuits in RF Systems, Austin, TX, Jan 2013*, pp. 171–173.
7. **Hong J-S and Lancaster MJ** (2001) Microstrip filters for rf/microwave applications. *IEEE Microwave Magazine* **3**, 62–65.
8. **Hung W, Chang C and Lee T** (2017) Real-time and noncontact impulse radio radar system for μm movement accuracy and vital-sign monitoring applications. *IEEE Sensors Journal*, **17**, 2349–2358.
9. **Kartal M, Golezani JJ and Doken B** (2017) A triple band frequency selective surface design for gsm systems by utilizing a novel synthetic resonator. *IEEE Transactions on Antennas and Propagation*, **65**, 2724–2727.
10. **Koshelev VI, Buyanov YI, Andreev YA, Plisko VV and Sukhushin KN** (2001) Ultrawideband radiators of high-power pulses. IEEE Conference Record - Abstracts. PPPS-2001 Pulsed Power Plasma Science 2001. 28th IEEE International Conference on Plasma Science and 13th IEEE International Pulsed Power Conference (Cat. No.01CH37), Las Vegas, NV, USA, 2001, pp. 509.
11. **Liang X, Zhang H, Fang G, Ye S and Gulliver TA** (2017) An improved algorithm for through-wall target detection using ultra-wideband impulse radar. *IEEE Access*, **5**, 22101–22118.
12. **Loubriel GM, Zutavern FJ, Baca AG, Hjalmarson HP, Plut TA, Helgeson WD, O'Malley MW, Ruebush MH and Brown DJ** (1997) Photoconductive semiconductor switches. *IEEE Transactions on Plasma Science*, **25**, 124–130.
13. **Pasya I, Mahyuni A, Adnan SFS and Awang Z** (2011) Analysis of interference from uwb radar signals on a digital ofdm transmission system. *2011 IEEE International Conference on System Engineering and Technology, Shah Alam, Jun 2011*, pp. 91–95.
14. **Proud JM and Norman SL** (1978) High-frequency waveform generation using optoelectronic switching in silicon. *IEEE Transactions on Microwave Theory and Techniques*, **26**, 137–140.
15. **Reineix G, Négrier R, Lalande M, Couderc V, Andrieu J and Desrumaux L** (2017) Optoelectronic waveforms generation: Pcss characterization and genetic algorithm. *2017 47th European Microwave Conference (EuMC), Nuremberg, Oct 2017*, pp. 1373–1376.
16. **Xiong X, Hong Weijun, Zhao Zhentao, Deng Li and Li Shufang** (2015) Wifi band-stop fss for increased privacy protection in smart building. *2015 IEEE 6th International Symposium on Microwave, Antenna, Propagation, and EMC Technologies (MAPE), Shanghai, Oct 2015*, pp. 826–828.
17. **Zhang S and Zhu L** (2012) Triple-mode bandpass filters on stub-loaded resonator with novel i/o coupling scheme. *2012 Asia Pacific Microwave Conference Proceedings, Kaohsiung, Dec 2012*, pp. 532–534.



Jeremy Hyvernaud received the Dipl.-Ing. degree in mechatronics from the Engineers School of Limoges, Limoges, France, in 2018. He is currently pursuing the Ph.D. degree from the XLIM Laboratory, University of Limoges, Limoges, France. His research interests include the development of transient signal generators incorporating optoelectronic devices for EMC applications.



Gwenael Reineix received the Dipl.-Ing. degree in mechatronics from the Engineers School of Limoges, Limoges, France, in 2016. He is currently pursuing the Ph.D. degree from the XLIM Laboratory, University of Limoges, Limoges, France. His research interests include waveforms generation based on optoelectronic generators for EMC and radar applications.



Romain Negrier received the Ph.D. degree in telecommunications engineering from the University of Limoges, Limoges, France, in 2016. For nearly a year, he was a Research Engineer with the Antennas and Microwave Devices Department, IETR, University of Nantes, France. He is currently an Associate Professor with the XLIM Research Institute, University of Limoges. His research interests include wireless sensor network, ultrawideband, and radar system.



Joel Andrieu received the Ph.D. degree in electronics from the University of Limoges, Limoges, France, in 1990. He is currently a Professor with the University of Limoges and Member of XLIM Research Institute, University of Limoges/National Center For Scientific Research (CNRS), Brive, France. His research interests include ultrawideband metrology for various applications, radar, EMCs, and HPMS.



Michele Lalande received the Ph.D. degree in electronics from the University of Limoges, Limoges, France, in 1986. She is currently a Professor with the University of Limoges and a Member of XLIM Research Institute, University of Limoges/National Center For Scientific Research (CNRS), Brive, France. Her research interests include the area of antennas, transient measurement applications, and ultra-

wideband metrology for radar and HPMS.



Vincent Couderc received the Ph.D. degree from the University of Limoges, Limoges, France. He is currently the Head of the Photonics Group, XLIM Research Institute, Limoges, France. His research interests include spatial solitons propagation, diode-pumped laser source, nonlinear frequency conversion, and optoelectronic switching. Dr. Couderc is a member of the French Optical Society.